Title

Interleukin-23 Regulates Inflammatory Osteoclastogenesis via Activation of CLEC5A(+) Osteoclast Precursors.

Journal

Arthritis & Rheumatology, 75(8)

Authors

Furuya, Hiroki

Nguyen, Cuong

Gu, Ran

et al.

Publication Date

2023-08-01

DOI

10.1002/art.42478

Peer reviewed

HHS Public Access

Author manuscript

Arthritis Rheumatol. Author manuscript; available in PMC 2024 August 01.

Published in final edited form as:

Arthritis Rheumatol. 2023 August ; 75(8): 1477–1489. doi:10.1002/art.42478.

IL-23 regulates inflammatory osteoclastogenesis via the activation of MDL-1^{+} osteoclast precursors

Hiroki Furuya, MD, PhD[1,#], **Cuong Thach Nguyen, PhD**[2,#], **Ran Gu, PhD**[2], **Shie-Liang Hsieh, MD, DPhil**[3], **Emanual Maverakis, MD**[4], **Iannis E Adamopoulos, MPhil, DPhil**[1,2,*]

[1]Department of Rheumatology, Beth Israel Deaconess Medical Center, Harvard Medical School,

[2]Division of Rheumatology, Allergy and Clinical Immunology, University of California at Davis,

[3]Genomics Research Center, Academia Sinica, 128 Academia Road, Section 2, Nankang, Taipei, Taiwan

[4]Department of Dermatology, University of California, Davis, Sacramento, CA, USA

Abstract

Objective: To investigate the role of Interleukin-23 (IL-23) in pathological bone remodeling in inflammatory arthritis.

Methods: In this study we investigate the role of IL-23 in osteoclast differentiation and activation using in vivo gene transfer techniques in WT and MDL-1 deficient mice and performing in vitro and in vivo osteoclastogenesis assays using spectral flow cytometry, micro-CT analysis, Western blotting and immunoprecipitations.

Results: Herein, we show that IL-23 induces the expansion of a myeloid osteoclast precursor population and supports osteoclastogenesis and bone resorption in inflammatory arthritis. Genetic ablation of C-type lectin domain family 5, member A (CLEC5A), also known as myeloid DNAX activation protein 12 (DAP12)-associating lectin-1 (MDL-1), prevents IL-23-induction of osteoclast precursors associated with bone destruction as commonly observed in inflammatory arthritis. Moreover, osteoclasts derived from the bone marrow of MDL-1 deficient mice showed impaired osteoclastogenesis and MDL-1$^{-/-}$ mice had increased bone mineral density.

Conclusion: Our data show that IL-23 signaling regulates the availability of osteoclast precursors in inflammatory arthritis that could be effectively targeted for the treatment of inflammatory bone loss in inflammatory arthritis.

Introduction

Interleukin-23 (IL-23) and its cognate receptor interleukin-23R (IL-23R):IL-12Rβ1 plays a critical role in the pathogenesis of many autoimmune diseases, including rheumatoid

[*]**Correspondence:** Iannis E. Adamopoulos, Division of Rheumatology, and Clinical Immunology, Harvard Medical School, Beth Israel Medical Deaconess Center, Boston, MA. Tel 617-735-4162. Iadamopo@bidmc.harvard.edu.
[#]Equal Contribution

Disclosures

The authors have no financial conflicts of interest.

arthritis, psoriasis and psoriatic arthritis. However how pathological bone remodeling is regulated in inflammatory arthritis remains elusive. Activation of receptor activator of nuclear factor k beta receptor (RANK) by its ligand (RANKL) regulates osteoclast differentiation together with co-stimulatory signals that are regulated by immunoreceptor tyrosine-based activation motifs (ITAM) present on myeloid cells (1, 2). Pathological bone resorption in inflammatory arthritis differs greatly from physiological bone resorption due to the inflammatory infiltrate within the joint which alters the availability and nature of osteoclast precursors and the activation of co-stimulatory pathways elicited by pro-inflammatory mediators (3–6). Co-stimulatory signals are regulated through two main ITAM-containing adaptors expressed by myeloid cells, the FcRγ and DNAX activation protein-12 (DAP12) which pair with at least 20-ITAM associated receptors in osteoclasts including c-fms, TREM, OSCAR, and MDL-1 to activate Syk downstream signaling and osteoclast differentiation (7, 8). The first identified pairing partner of DAP12 is MDL-1 (myeloid DAP12-binding protein-1, also known as C-type lectin family member 5A or CLEC5A), a member of the NK cell receptor-like subfamily of C-type lectins (9). MDL-1 is expressed exclusively on myeloid cells and is a major PU.1 transcriptional target during myeloid differentiation regulating a number of myeloid-dependent immune and inflammatory responses including differentiation, activation and recruitment of myeloid cells during inflammation (10–13).

We and others have previously shown that MDL-1 is involved in autoimmune arthritis and osteoclast differentiation via its association with DAP12 (14–17). Interestingly the $DAP12^{+}/MDL\text{-}1^{+}$ population is significantly enriched in the $CD16^{+}$ PBMC fraction in humans (15), previously associated with bone destruction in PsA (18). Other studies have showed that MDL-1 is important in osteoclastogenesis and the formation of neutrophil extracellular trap (NET), as well as the development of $\gamma\delta$ T cells (19–21) which have clinically a pathogenic role in PsA and affect multiple tissues including skin and joints (22). To date, no endogenous physiological ligand or counter-receptor has been described for MDL-1 aside from the dengue virus interaction which stimulate the release of macrophage pro-inflammatory cytokines (20).

Thus, in this study we sought to identify mechanistically the role of MDL-1 in IL-23-induced inflammation and osteoclastogenesis. Herein, using state-of-the-art transgenic and molecular approaches, we demonstrate a novel functional interaction between IL-23 signaling and MDL-1 associated with the development of bone destruction *in vitro* and *in vivo*. Collectively, our data demonstrate that IL-23 signaling elicits the differentiation of MDL-1+ monocytes that serve as osteoclast precursors in inflammatory arthritis, suggesting that therapeutic strategies targeting MDL-1 may be beneficial in combating inflammatory bone loss as commonly observed in inflammatory arthritis.

Methods:

Animals

C57BL/6 and $Rag^{-/-}$ mice (8–12 weeks-old) were purchased from Jackson Laboratories (Sacramento, CA). IL-$23R^{GFP+/+}$ and $Mdl\text{-}1^{-/-}$ mice were obtained from Dr. Kuchroo (Harvard Medical School) and Dr. Hsieh (National Yang-Ming University, Taiwan),

respectively as previously described (20, 23). IL-23R$^{GFP+/+}$ *Rag*$^{-/-}$ mice were generated by crossing IL-23R$^{GFP+/+}$ reporter mice with *Rag*$^{-/-}$ mice as previously described (23). Sex- and age-matched mice at 26 weeks of age was used for micro-computer tomography analysis, and 8–12 weeks of age were used for all the other experiments and kept under specific pathogen-free conditions.

Reagents

Monoclonal antibodies of anti-Ly6G (1A8, FITC), MDL-1 (226402, AF405 and PE) were purchased from R&D Systems (Minneapolis, MN), CD11b (M1/70) and from ebioscience and CXC3R1 (SA011F11, BV711), B220 (RA3–6B2, PE/Dazzle594), Ter119 (TER-119, APC/Cyanine7), CSF1R (AFS98, BV605), Ly6C (HK1.4, BV510), CD61 (2C9.G2, PE), CD45 (30-F11, PerCP/Cyanine 5.5), RANK (R12–31, APC) and CD11c (N418, BV605) from BioLegend (USA). IL-23 ELISA kits were purchased from eBioscience, and RANKL and OPG ELISA kits were purchased from R&D Systems.

Production and purification of GFP, IL-23 and RANKL minicircle DNA and hydrodynamic delivery

Minicircle-RSV.Flag.mIL23.elasti.bpA, RSV.eGFP.bpA and RSV.mRANKL.bpA were produced as described by Chen *et al* (24). Briefly, a single isolated colony was grown in Luria–Bertani broth supplemented with kanamycin. Overnight cultures were centrifuged at 20°C, 4000 rpm for 20 min. The pellet bacteria were incubated at 32°C with constant shaking at 250 rpm for 2 h. Episomal DNA minicircles (MC) were prepared from bacteria using EndoFreeMegaprep plasmid purification kits (Qiagen). Fifteen micrograms of RANKL, IL-23 or GFP MC DNA was injected hydrodynamically via tail vein delivery. Murine serum 1-day post gene transfer was collected for ELISA serum RANKL and IL-23, as previously described (14, 25).

Spectral Flow cytometry and high-dimensional analysis

Bone marrow (BM) cells were flushed out using a 27-gauge needle attached to a 1 ml syringe containing PBS. Gates were established using B220^{-}CD3^{-}Ter119^{-} to select the negative population and then an additional gate selecting the c-fms+ cells ensured the selection of the myeloid fraction.

Among B220^{-}CD3^{-}Ter119^{-}CSF1R^{+} myeloid precursor cells, clustering algorithm was conducted by FlowSOM based on the marker expression of CD11c, CD61, CD11b, CX3CR1, RANK, MDL1, Ly6G, CD45, Ly6C on all cells, and the size of each pie slices show the expression levels of each molecule. As this method is highly sensitive and vulnerable to batch effect, FlowSOM were conducted on single experiment using to avoid confounding bias (26). The FlowSOM clusters was also displayed on top of the t-SNE axes to visualize each cluster. All events were captured by an Cytek Aurora cytometer and analyzed with FlowJo software version 10.

Osteoclast, osteoblast cultures and functional assays

Bone marrow cells were cultured in α-MEM in the presence of M-CSF (25 ng/mL) for 2 days then with M-CSF (25 ng/mL) and RANKL (30 ng/mL) for 2, 4, or 8 days

as indicated in individual experiments. Functional assessment of osteoclast formation was performed by TRAP staining, F-actin ring staining, expression of osteoclast related genes, bone resorption assays, and scanning electron microscopy as previously described (27). Confocal microscopy of BMMs and osteoclasts was performed on cells fixed on coverslips with 4% paraformaldehyde in PBS for 20 minutes, followed by incubation with PBS/0.2% BSA/0.1% Saponin for 30 minutes followed by incubation with appropriate antibodies. Immunofluorescence-labeled cells were observed using a Nikon Confocal Microscope C1. For *in vitro* osteoclast deacetylation functional assay, BMM stimulated with MCSF+RANKL were placed on ice under a Zeiss AxioObserver fluorescent microscope equipped with Photometrics CoolSnap HQ camera and Definite Focus attachment for time-lapse stability. Images were acquired at 5, 10, 15, 30 and 60 minutes. For osteoblast cultures calvaria-derived cells were isolated from pups (1–3 days old) by three sequential collagenase/dispase digestions, and treated with ascorbic acid (ASC), and dexamethasone (Dex) (50 μM ascorbate-2-phosphate, 10 μM B(beta)-glycerophosphate and 0.1 μM dexamethasone) as previously shown (28). Alkaline phosphatase was detected using a commercial kit (Sigma-Aldrich) according to the manufacture's protocol and the mineralized bone matrix was stained with 2% Alizarin Red (pH 4.1–4.3) (Sigma-Aldrich) in osteoblasts fixed in 10% formaldehyde. Bone resorption pit depth was measured as previously described (29).

Micro-computer tomography (μCT)

Tibias were amputated from WT (n=7) and *Mdl-1*$^{-/-}$ (n=14) mice at 26 weeks of age. The specimens were fixed in cold 10% neutral buffered formalin until processing. High-resolution μCT scans of mouse tibias were scanned at Numira Biosciences (Salt Lake City, UT) using a high-resolution volumetric μCT40 scanner (Scanco Medical AG, Bassersdorf, Switzerland). The image data were acquired at 6-μm isometric voxel resolution at 300 ms exposure time, 2000 views, and five frames per view. The μCT-generated DICOM files were used to analyze the samples and to create volume renderings of the region of interest. The raw data files were viewed using Microview (GE Healthcare, Milwaukee, WI, USA). Using ScanCo Medical software, we obtained bone density measurements for the femur's midshaft and distal end. For distal femur analysis, a three-dimensional trabecular volume (TV) was selected 0.5 mm below the growth plate and 0.5 mm thick. For midshaft analysis, the length of the entire femur was measured, and a 1-mm-thick midcortical section was used for analysis. A threshold of 20% of the 16-bit total grayscale values between 0 and 32,000 was used. Original volumetric reconstructed were used to generate three-dimensional image rendering through images using Microview software (GE Healthcare, Piscataway, NJ, USA). Bone histomorphometry was performed as previously described (14).

Western blotting and Immunoprecipitation

Bone marrow macrophages were treated with mouse recombinant IL-23 for 0, 5, 15, 45 min. After incubation, the cells were washed two times with ice-cold D-PBS, and lysed with cell lysis buffer (50 mM Tris-HCl (pH 7.4), 150 mM NaCl, 1 mM EDTA, 1% Triton X-100, 1 mM PMSF, 1 mM Na_3VO_4, 1 mM NaF) on ice for 15 min. Protein concentration was determined by Pierce BCA Protein Assay as manufacturer's instructions. 30–100 μg of proteins were separated on SDS–PAGE and transferred onto a PVDF membrane.

Immunoprecipitation (IP) experiments were performed using protein-G Dynabeads® as manufacturer's instructions with minor modification. Briefly, protein G-Dynabeads were incubated with the appropriate specific antibody for 1 hr at 4°C. Cell lysates were incubated with the Protein G-Dynabeads-appropriate specific antibody complex for over 2 hr at 4°C. After third-time washing, immunoprecipitated protein lysates (IP complex) and whole cell lysates (input) were separated on SDS–PAGE and transferred onto a PVDF membrane. The membranes were blocked with 5 % skim milk at room temperature for one hour and incubated with the appropriate primary antibodies at 4°C overnight. Next, the membranes were incubated with IRDye® 680CW appropriate secondary antibodies. Immunoreactive bands were detected by Odyssey® Imaging Systems.

Statistical analysis

Statistical differences were analyzed by Mann–Whitney test. All results are representative of 3 independent experiments. Statistically significant differences were considered as $P < 0.05$ ($^{*}P < 0.05$, $^{**}P < 0.01$, $^{***}P < 0.001$). All statistical analyses were performed using GraphPad Prism software.

Study approval

All animal protocols (protocol #20010 and #20845) were approved by Institutional Animal Care and Use Committee, at Beth Israel Medical Deaconess Center and University of California at Davis. All experiments were performed in accordance with relevant guidelines and regulations.

Results

IL-23 induces the expansion of MDL-1^{+} osteoclast precursors

To identify the effect of IL-23 in bone remodeling we performed IL-23 gene transfer in C57BL/6 mice and compared it with RANKL and GFP control as previously described (30). To analyze the effect of IL-23 on osteoclast precursors we performed spectral cytometry on bone marrow cells isolated six days post-GFP/RANKL/IL-23 gene transfer using an extensive panel of myeloid-specific antibodies (Figure 1A). We focused our analysis on myeloid precursors by gating on the B220, CD3, Ter119 negative and c-fms positive population (Figure 1B). Among this myeloid population, we integrated the data of GFP/RANKL/IL-23 gene transfer and conducted an unsupervised clustering algorithm with a combination of tSNE and FlowSOM (flow cytometry data analysis using self-organizing maps), showing 10 distinct populations (Figure 1C, D). The clustering was based on the expression level of CD11c, CD61 (b3-integrin), CD11b, CX3CR1 (C-X3-C Motif Chemokine Receptor 1), RANK, MDL-1, Ly6G, CD45 and Ly6C. The expression levels of each molecule are graphically represented by the size of each pie slices among each cluster (Figure 1D). Our data demonstrated that RANKL and IL-23 induce unique alterations in the myeloid populations by dissecting the origin of the t-SNE mapping (Figure 1E). Next, we gated on the CSF1R^{+}LY6G^{-} cells to remove neutrophils from our analysis and gated on CSF1R^{+}CD11b^{+}LY6C^{+} to focus on inflammatory monocytes and identified two distinct CX3CR1^{high} monocyte populations that include CD11c^{-} and CD11c^{+} monocytes according to the FlowSOM clustering and confirmed these populations by flow cytometry

(Figure 1D, F). IL-23 but not RANKL significantly induced the expansion of MDL-1^+ cells (Figure 1G), and both RANKL and IL-23 induced the expansion of inflammatory monocytes $LY6C^+CX3CR1^{low}$ (Figure 1H). We also detected a significant increase on RANK expression in the $CD11c^+$ monocytes population suggesting that IL-23 regulates the osteoclast precursor population of MDL-1^+ inflammatory monocytes (Figure 1I).

IL-23 activates inflammatory DAP12 signaling in MDL-1^+ IL-$23R^+$ double positive cells

Next, we investigated the expression of IL-23R and MDL-1 in macrophages and osteoclasts by utilizing the IL-23R reporter mice (IL-$23R^{GFP+/+}$) where the intracellular domain of IL-23R is replaced with an internal ribosome entry site (IRES)- green fluorescent protein (GFP) which is used for detection of IL-23R (31). Thus, using fluorescence microscopy, we demonstrated that IL-23R and MDL-1 were co-expressed in macrophages and osteoclasts derived from IL-$23R^{GFP+/+}$ and IL-$23R^{GFP+/+}$*Rag*$^{-/-}$ mice using anti-GFP antibody for IL-23R (IL-$23R^{GFP+/+}$) and anti-MDL-1 respectively (Figure 2A). Next by using the homozygous IL-23R reporter mice (IL-$23R^{GFP+/+}$) we effectively blocked all IL-23R downstream signaling similar to IL-23R deficient mice and used these mice to test IL-23 signaling via the MDL-1- DAP12 complex. We performed immunoprecipitations with anti-DAP12 antibody using total cell lysate of BMM derived from IL-$23R^{GFP+/+}$ and *Mdl-1*$^{-/-}$ mice stimulated with 100 ng/ml of mouse rIL-23. Our data showed that upon IL-23 stimulation, DAP12 co-immunoprecipitated with MDL-1, IL-23R, and SYK in WT mice (Figure 2B). Interestingly, no binding with DAP12 was observed with MDL-1 in IL-$23R^{GFP+/+}$ mice and with IL-23R in *Mdl-1*$^{-/-}$ mice, suggesting a functional interaction between the two receptors. Syk binding was inhibited, albeit not abolished in *Mdl-1*$^{-/-}$ and IL-$23R^{GFP+/+}$ mice (Figure 2B) as tonic DAP12 ITAM signaling is not disturbed in these mice. Next, we confirmed these observations by performing MDL-1 immunoprecipitations and probing with DAP12, MDL-1, IL-23R, and SYK (Figure 2C). Taken together our data demonstrate that IL-23R and MDL-1 form large protein assemblies to transduce co-stimulatory signals resulting in the activation of SYK during inflammatory osteoclastogenesis.

MDL-1 regulates the myeloid PU.1 transcriptional program in RANKL signaling.

In keeping with previous reports indicating that MDL-1 is a specific myeloid lineage marker, expression of *Mdl-1* was increased during myeloid differentiation assays (osteoclastogenesis) evidenced by the formation of multinucleated $TRAP^+$ cells in RANKL-induced bone marrow cultures (Figure 3A, B) but not during osteoblast maturation, indicated by Alkaline phosphatase (Alp) and Alzarin-red staining as well as bone sialoprotein (Bsp) positivity at day 14 and 21 (Figure 3C–E). These data collectively prompted us to investigate the role of MDL-1 in osteoclastogenesis and its contribution in skeletal homeostasis.
In order to explore the effect of MDL-1 in osteoclast precursors we performed DNA microarray analysis and compared WT and *Mdl-1*$^{-/-}$ macrophages stimulated for 4 days with M-CSF (day 4). Out of the 30,854 detected genes, we identified a total of 1,607 genes that were significantly different and displayed $\log_2$ fold changes > 2.0 and adjusted *P*-values < 0.001 and these genes were selected for further analysis between WT and *Mdl-1*$^{-/-}$ macrophages. The identified differentially expressed genes (DEGs) are involved in osteoclastogenesis (*Mmp9*, *Acp5, CtsK*, *C-fos, Nfatc1, Nfkb)*, inflammatory response (*Saa3*,

Cd83, *Cd86, Socs3*), pro-inflammatory cytokines and chemokines (*Il-1β*, *Cxcl-9*, *Cxcl-10*) and neutrophil activation (*Csf3r, Fpr2, Mpo)*. In keeping with the concept that MDL-1 is a major transcriptional target for the myeloid master regulator PU.1, 376 genes were identified in BMMs stimulated with MCSF to be critically involved in PU.1 signaling pathway and in cell cycle and anti-apoptosis (*Cdca2*, *Cdc20*, *Lmnb1*, *Pik*, and *Mad2l1*,) and cell survival (*Ccl5*, *Pla2g7*) of macrophages by using the Ingenuity® Pathway Analysis (IPA®) (Figure 3E, F). To evaluate the functional significance of the identified DEGs, we performed quantitative cell cytotoxicity and viability assays using Calcein-live//EthD1 fluorescent staining and resazurin as a fluorometric/colorimetric growth indicator, respectively and demonstrated that *Mdl-1*$^{-/-}$ macrophages had an overall lower survival than WT control macrophages (Figure 3G, H). Next, we performed phosphorylation assays of Erk, Akt, and NF-κB in total cell lysates of BM derived macrophages from WT, and *Mdl-1*$^{-/-}$ stimulated with mouse rIL-23 (100 ng/ml) for 0, 5, 15, 45 mins. IL-23 induced phosphorylation of Erk, Akt, and NF-κB in WT macrophages; however, it was significantly suppressed in *Mdl-1*$^{-/-}$ macrophages at 5, 15, and 45 min post-treatment, compared to WT macrophages (Figure 3I). The data were significant even when normalized to a housekeeping protein (Figure 3J).

MDL-1 deficiency impairs osteoclast differentiation and bone resorption

Next, we investigated the role of MDL-1 in osteoclast differentiation using functional assays. Specifically, to investigate whether MDL-1 deficiency influences osteoclastogenesis, BMM cells derived from WT and *Mdl-1*$^{-/-}$ mice were cultured in the presence of RANKL for 2, 3, 4 days. We observed delayed osteoclast maturation in *Mdl-1*$^{-/-}$ mice as evidenced by the formation of fewer multinucleated TRAP^{+} cells and a lower total number of osteoclasts (TRAP^{+}) (Figure 4A, B). These findings correlated with reduced gene expression of *Acp5* and other osteoclast markers including *Ctsk* and *Mmp9* (Figure 4C–E). Most importantly, gene expression of osteoclast precursor markers *C-fms*, *C-fos*, *Nfatc1,* and *Tnfrsf11a* were also significantly reduced in bone marrow derived cultures stimulated with MCSF at an early time-point (day 4) and MSCF + RANKL at a late time-point (day 8) compared to WT osteoclasts (Figure 4F). Consistent with the findings outlined above, MDL-1 deficient osteoclasts exhibited reduced bone resorption on dentine slices in both resorbed surface area (Figure 4G) and depth (Figure 4H) compared to WT osteoclasts. Next, we investigated the role of IL-23 in in-vitro osteoclastogenesis assays in the presence of sub-optimal levels of RANKL. Again, there was as significant delay in osteoclastogenesis that was not rescued with IL-23 as evidenced by the TRAP staining and osteoclast-related markers (Figure 4I–M), suggesting that IL-23 stimulation is not sufficient to rescue osteoclastogenesis in MDL-1$^{-/-}$ mice *in vitro*.

MDL-1 deficient mice have increased bone mineral density

To determine the physiological roles of MDL-1 in homeostatic skeletal remodeling, we performed micro-computed tomography (μCT) analysis of distal femoral trabecular and compared between WT and *Mdl-1*$^{-/-}$ mice (Figure 5A). We found that the *Mdl-1*$^{-/-}$ mice had significantly higher cancellous bone volume at the distal femoral metaphysis with thicker trabecular than WT mice (Figure 5B, C). Specifically, the trabecular bone/tissue volume ratio (BV/TV) was significantly increased in *Mdl-1*$^{-/-}$ mice, by more than 200% (Figure 5D) and accompanied by 19% increase in trabecular number (Tb.N) (Figure 5E),

34% increased trabecular thickness (Tb.Th) (Figure 5F), and a 175% increase in bone surface (B.S) (Figure 5G) compared to WT controls.

Consistent with the increased bone mass observed by μCT analysis, bone histomorphometry analysis of *Mdl-1*$^{-/-}$ mice also showed lower osteoclast surface over bone surface area (Oc.S/BS) (Figure 5H). These changes were also accompanied by significantly lower levels (52%) of serum C-terminal telopeptide fragments of the type I collagen (CTX-1) levels (bone resorption marker) in *Mdl-1*$^{-/-}$ mice compared to WT control mice (Figure 5I), consistent with a previous report (32). Accordingly, bone histomorphometry analysis of *Mdl-1*$^{-/-}$ mice (Figure 5J, K) also showed increased calcium deposits in *Mdl-1*$^{-/-}$ mice which was independent of changes in serum RANKL concentration and/or RANKL/OPG ratio (Figure 5L–N).

Discussion

IL-23 is regulating the expansion of Th17 cells and is implicated in inflammatory arthritis and bone destruction via the activation of NF-kB which is the target of RANKL (33, 34). However, the dysregulation of bone remodeling in inflammatory arthritis has been extensively studied as it relates to pathogenic Th17 cells. Th17 cells have the ability to modulate RANK-signaling either by secreting RANKL directly (35), or by influencing the expression of RANKL by stromal cells and RANK by osteoclast precursors via IL-17 signaling (25, 36, 37). However, Th17 cells are not predominant in the inflamed joints of arthritis patients, and IL-17 seem to modulate RANK-expression only in certain myeloid populations (38, 39). Therefore, pathological bone remodeling in inflammatory arthritis may utilize alternative pathways of osteoclast differentiation. However, how IL-23 affects RANKL-bone remodeling in inflammatory arthritis has not been fully elucidated.

Herein we show that IL-23 induces the expansion of MDL-1^{+} in c-fms^{+}CX3CR1^{+} inflammatory monocytes which are known to be a population of inflammatory osteoclast precursors identified *in vitro* and *in vivo* in inflamed synovium (40, 41). Moreover, we show that IL-23R and MDL-1 receptors are expressed in pre-osteoclasts and osteoclasts and participate in the activation of DAP12 co-stimulatory pathway of osteoclastogenesis (Figure 6). DAP12 is a transmembrane protein with a minimal extracellular domain, which relies on the association of other cell surface receptors to transduce its signals to an ITAM in its cytoplasmic tail. Neither DAP12 nor many of its associated receptors can efficiently reach the cell surface alone, and DAP12 is required for their signaling abilities (8, 42). IL-23 induces the expansion of MDL-1 and thus DAP12-costimulatory signaling. It is also possible that in inflammatory conditions IL-23 can induce a specific subset of osteoclast precursors such as LY6C^{+}CD11c^{+} monocytes, which is known as inflammatory osteoclast precursors (43, 44). Since IL-23 induces RANK expression in this population we cannot confirm a RANKL-independent action of IL-23 in osteoclast differentiation. This would require further work on RANK deficient mice, however this is a moot point as all inflammatory arthritis patients have active signaling to some degree. Although there was no significant difference in serum RANKL/OPG levels between MDL-1$^{-/-}$ and WT, these data still require careful interpretation since there may be difference between systemic and local RANKL level. Additionally although the ratio between RANKL and OPG remain unaltered other

factors such as TRAIL can also modulate availability of RANKL by sequestering OPG (45). There are many TRAIL targets in inflammation and hence there is no absolute standard to measure utility of this pathway from serum.

In our experiments in the MDL-$1^{-/-}$ it was the availability of osteoclast precursors that affected the osteoclastogenesis and bone resorption *in vitro* and *in vivo*. Although IL-23 induces the MDL-1^{+} inflammatory monocytes which serve as osteoclast precursors in inflammatory arthritis, MDL-1 has also roles in physiological bone remodeling. It was previously shown that MDL-1 together with DAP10 and DAP12 form a multi-protein assembly complex that harbors ITAM/YINM stimulatory/costimulatory motifs and thus can regulate osteoclastogenesis (17). Moreover, we have previously shown in human PBMC that cells that are double positive for MDL-1 and DAP12 are not in the $CD16^{+}$ cell fraction rather than $CD14^{+}$ suggesting that these pathways may be more important in specific cell types (46). In keeping with this notion psoriatic arthritis patients who have higher levels of IL-23 have also higher number of circulating $CD16^{+}$ osteoclast precursors and increased CD16 expression was associated with a higher bone erosion activity in PsA (47). On the contrary, in rheumatoid arthritis patients the main osteoclast precursors seem to be identified in the $CD14^{+}CD16^{-}$ fraction (48). Thus, these data suggest that alternative osteoclast differentiation pathways may occur in different arthritis patients depending on both the pathological pro-inflammatory signals and the unique inflammatory osteoclast precursors.

Additionally, as others have previously demonstrated that DAP12-ITAM mediated signaling is required for integrin signaling in neutrophils (49), -associated with skin inflammation in PsA-, and the IL-23R co-receptor IL-12Rβ1 also regulates many classes of ITAM-bearing receptors in NK and T cells resulting in potent co-stimulatory signals (50, 51), it is anticipated that this pathway will have wider significance beyond inflammatory osteoclastogenesis

Financial support

This work was supported by National Institutes of Health/National Institute of Arthritis and Musculoskeletal and Skin Diseases Grant 2R01AR062173 grant to IEA.

References

1. Boyle WJ, Simonet WS, Lacey DL. Osteoclast differentiation and activation. Nature.2003;423(6937):337–42. [PubMed: 12748652]
2. Koga T, Inui M, Inoue K, Kim S, Suematsu A, Kobayashi E, et al. Costimulatory signals mediated by the ITAM motif cooperate with RANKL for bone homeostasis. Nature. 2004;428(6984):758–63. [PubMed: 15085135]
3. O'Brien W, Fissel BM, Maeda Y, Yan J, Ge X, Gravallese EM, et al. RANK-Independent Osteoclast Formation and Bone Erosion in Inflammatory Arthritis. Arthritis Rheumatol. 2016;68(12):2889–900. [PubMed: 27563728]
4. Yao Z, Xing L, Boyce BF. NFkB p100 limits TNF-induced bone resorption in mice by a TRAF3-dependent mechanism. The Journal of Clinical Investigation. 2009;119(10):3024–34. [PubMed: 19770515]
5. Dickerson TJ, Suzuki E, Stanecki C, Shin HS, Qui H, Adamopoulos IE. Rheumatoid and pyrophosphate arthritis synovial fibroblasts induce osteoclastogenesis independently of RANKL, TNF and IL-6. Journal of autoimmunity. 2012;39(4):369–76. [PubMed: 22867712]

6. Otero JE, Dai S, Alhawagri MA, Darwech I, Abu-Amer Y. IKKbeta activation is sufficient for RANK-independent osteoclast differentiation and osteolysis. Journal of bone and mineral research : the official journal of the American Society for Bone and Mineral Research. 2010;25(6):1282–94. [PubMed: 20200955]
7. Ivashkiv LB. Cross-regulation of signaling by ITAM-associated receptors. Nat Immunol. 2009;10(4):340–7. [PubMed: 19295630]
8. Hamerman JA, Ni M, Killebrew JR, Chu C-L, Lowell CA. The expanding roles of ITAM adapters FcRγ and DAP12 in myeloid cells. Immunological Reviews. 2009;232(1):42–58. [PubMed: 19909355]
9. Bakker AB, Baker E, Sutherland GR, Phillips JH, Lanier LL. Myeloid DAP12-associating lectin (MDL)-1 is a cell surface receptor involved in the activation of myeloid cells. Proc Natl Acad Sci U S A. 1999;96(17):9792–6. [PubMed: 10449773]
10. Aoki N, Kimura Y, Kimura S, Nagato T, Azumi M, Kobayashi H, et al. Expression and functional role of MDL-1 (CLEC5A) in mouse myeloid lineage cells. J Leukoc Biol. 2009;85(3):508–17. [PubMed: 19074552]
11. Batliner J, Mancarelli MM, Jenal M, Reddy VA, Fey MF, Torbett BE, et al. CLEC5A (MDL-1) is a novel PU.1 transcriptional target during myeloid differentiation. Mol Immunol. 2011;48(4):714–9. [PubMed: 21094529]
12. Gingras M-C, Lapillonne H, Margolin JF. TREM-1, MDL-1, and DAP12 expression is associated with a mature stage of myeloid development. Mol Immunol. 2002;38(11):817–24. [PubMed: 11922939]
13. Yim D, Jie H-B, Sotiriadis J, Kim Y-S, Kim YB. Molecular cloning and expression pattern of porcine myeloid DAP12-associating lectin-1. Cell Immunol. 2001;209(1):42–8. [PubMed: 11414735]
14. Adamopoulos IE, Tessmer M, Chao CC, Adda S, Gorman D, Petro M, et al. IL-23 is critical for induction of arthritis, osteoclast formation, and maintenance of bone mass. J Immunol. 2011;187(2):951–9. [PubMed: 21670317]
15. Shin H-S, Sarin R, Dixit N, Wu J, Gershwin ME, Bowman EP, et al. Crosstalk among interleukin 23 and DNAX activating protein 12-dependent pathways promotes osteoclastogenesis. J Immunol. 2015;194(1):316–24. [PubMed: 25452564]
16. Joyce-Shaikh B, Bigler ME, Chao CC, Murphy EE, Blumenschein WM, Adamopoulos IE, et al. Myeloid DAP12-associating lectin (MDL)-1 regulates synovial inflammation and bone erosion associated with autoimmune arthritis. J Exp Med. 2010;207(3):579–89. [PubMed: 20212065]
17. Inui M, Kikuchi Y, Aoki N, Endo S, Maeda T, Sugahara-Tobinai A, et al. Signal adaptor DAP10 associates with MDL-1 and triggers osteoclastogenesis in cooperation with DAP12. Proc Natl Acad Sci U S A. 2009;106(12):4816–21. [PubMed: 19251634]
18. Ritchlin CT, Haas-Smith SA, Li P, Hicks DG, Schwarz EM. Mechanisms of TNF-alpha- and RANKL-mediated osteoclastogenesis and bone resorption in psoriatic arthritis. The Journal of clinical investigation. 2003;111(6):821–31. [PubMed: 12639988]
19. Inui M, Kikuchi Y, Aoki N, Endo S, Maeda T, Sugahara-Tobinai A, et al. Signal adaptor DAP10 associates with MDL-1 and triggers osteoclastogenesis in cooperation with DAP12. Proc Natl Acad Sci U S A. 2009;106(12):4816–21. [PubMed: 19251634]
20. Chen ST, Lin YL, Huang MT, Wu MF, Cheng SC, Lei HY, et al. CLEC5A is critical for dengue-virus-induced lethal disease. Nature. 2008;453(7195):672–6. [PubMed: 18496526]
21. Chen S-T, Li F-J, Hsu T-y Liang S-M, Yeh Y-C, Liao W-Y, et al. CLEC5A is a critical receptor in innate immunity against Listeria infection. Nat Commun. 2017;8(1):299. [PubMed: 28824166]
22. Ritchlin CT, Colbert RA, Gladman DD. Psoriatic arthritis. N Engl J Med. 2017;376(10):957–70. [PubMed: 28273019]
23. Awasthi A, Riol-Blanco L, Jäger A, Korn T, Pot C, Galileos G, et al. Cutting edge: IL-23 receptor gfp reporter mice reveal distinct populations of IL-17-producing cells. J Immunol. 2009;182(10):5904–8. [PubMed: 19414740]
24. Chen Z-Y, He C-Y, Kay DMA. Improved production and purification of minicircle DNA vector free of plasmid bacterial sequences and capable of persistent transgene expression in vivo. Hum Gene Ther. 2005;16(1):126–31. [PubMed: 15703495]

25. Adamopoulos IE, Suzuki E, Chao CC, Gorman D, Adda S, Maverakis E, et al. IL-17A gene transfer induces bone loss and epidermal hyperplasia associated with psoriatic arthritis. Ann Rheum Dis. 2015;74(6):1284–92. [PubMed: 24567524]
26. Quintelier K, Couckuyt A, Emmaneel A, Aerts J, Saeys Y, Van Gassen S. Analyzing high-dimensional cytometry data using FlowSOM. Nat Protoc. 2021;16(8):3775–801. [PubMed: 34172973]
27. Adamopoulos IE, Sabokbar A, Wordsworth B, Carr A, Ferguson D, Athanasou N. Synovial fluid macrophages are capable of osteoclast formation and resorption. J Pathol. 2006;208(1):35–43. [PubMed: 16278818]
28. Wu DJ, Gu R, Sarin R, Zavodovskaya R, Chen CP, Christiansen BA, et al. Autophagy-linked FYVE containing protein WDFY3 interacts with TRAF6 and modulates RANKL-induced osteoclastogenesis. J Autoimmun. 2016;73:73–84. [PubMed: 27330028]
29. Parikka V, Lehenkari P, Sassi ML, Halleen J, Risteli J, Härkönen P, et al. Estrogen reduces the depth of resorption pits by disturbing the organic bone matrix degradation activity of mature osteoclasts. Endocrinology. 2001;142(12):5371–8. [PubMed: 11713237]
30. Adamopoulos IE, Tessmer M, Chao CC, Adda S, Gorman D, Petro M, et al. IL-23 is critical for induction of arthritis, osteoclast formation, and maintenance of bone mass. Journal of immunology. 2011;187(2):951–9.
31. Awasthi AR-BL, Jäger A, Korn T, Pot C, Galileos G, Bettelli E, Kuchroo VK, Oukka M. Cutting edge: IL-23 receptor gfp reporter mice reveal distinct populations of IL-17-producing cells. J Immunol. 2009;182(10):5904–8. [PubMed: 19414740]
32. Huang Y-L, Chen S-T, Liu R-S, Chen Y-H, Lin C-Y, Huang C-H, et al. CLEC5A is critical for dengue virus-induced osteoclast activation and bone homeostasis. J Mol Med 2016;94(9):1025–37. [PubMed: 27033255]
33. Rahman P, Inman RD, Maksymowych WP, Reeve JP, Peddle L, Gladman DD. Association of Interleukin 23 Receptor Variants with Psoriatic Arthritis. J Rheumatol. 2009;36(1):137–40. [PubMed: 19040306]
34. Nair RP, Duffin KC, Helms C, Ding J, Stuart PE, Goldgar D, et al. Genome-wide scan reveals association of psoriasis with IL-23 and NF-kappaB pathways. Nat Genet. 2009;41(2):199–204. [PubMed: 19169254]
35. Sato K, Suematsu A, Okamoto K, Yamaguchi A, Morishita Y, Kadono Y, et al. Th17 functions as an osteoclastogenic helper T cell subset that links T cell activation and bone destruction. The Journal of experimental medicine. 2006;203(12):2673–82. [PubMed: 17088434]
36. Kotake S, Udagawa N, Takahashi N, Matsuzaki K, Itoh K, Ishiyama S, et al. IL-17 in synovial fluids from patients with rheumatoid arthritis is a potent stimulator of osteoclastogenesis. The Journal of clinical investigation. 1999;103(9):1345–52. [PubMed: 10225978]
37. Adamopoulos IE, Chao CC, Geissler R, Laface D, Blumenschein W, Iwakura Y, et al. Interleukin-17A upregulates receptor activator of NF-kappaB on osteoclast precursors. Arthritis Res Ther. 2010;12(1):R29. [PubMed: 20167120]
38. Yamada H, Nakashima Y, Okazaki K, Mawatari T, Fukushi J-I, Kaibara N, et al. Th1 but not Th17 cells predominate in the joints of patients with rheumatoid arthritis. Ann Rheum Dis. 2008;67(9):1299–304. [PubMed: 18063670]
39. Sprangers S, Schoenmaker T, Cao Y, Everts V, de Vries TJ. Different Blood-Borne Human Osteoclast Precursors Respond in Distinct Ways to IL-17A. J Cell Physiol. 2016;231(6):1249–60. [PubMed: 26491867]
40. Madel MB, Ibanez L, Ciucci T, Halper J, Rouleau M, Boutin A, et al. Dissecting the phenotypic and functional heterogeneity of mouse inflammatory osteoclasts by the expression of Cx3cr1. Elife. 2020;9.
41. Hasegawa T, Kikuta J, Sudo T, Matsuura Y, Matsui T, Simmons S, et al. Identification of a novel arthritis-associated osteoclast precursor macrophage regulated by FoxM1. Nat Immunol. 2019;20(12):1631–43. [PubMed: 31740799]
42. Hamerman JA, Tchao NK, Lowell CA, Lanier LL. Enhanced Toll-like receptor responses in the absence of signaling adaptor DAP12. Nat Immunol. 2005;6(6):579–86. [PubMed: 15895090]

43. Ibanez L, Abou-Ezzi G, Ciucci T, Amiot V, Belaid N, Obino D, et al. Inflammatory Osteoclasts Prime TNFalpha-Producing CD4(+) T Cells and Express CX3 CR1. J Bone Miner Res. 2016;31(10):1899–908. [PubMed: 27161765]
44. Narisawa M, Kubo S, Okada Y, Yamagata K, Nakayamada S, Sakata K, et al. Human dendritic cell-derived osteoclasts with high bone resorption capacity and T cell stimulation ability. Bone. 2021;142:115616. [PubMed: 32866681]
45. Emery JG, McDonnell P, Burke MB, Deen KC, Lyn S, Silverman C, et al. Osteoprotegerin is a receptor for the cytotoxic ligand TRAIL. J Biol Chem. 1998;273(23):14363–7. [PubMed: 9603945]
46. Shin HS, Sarin R, Dixit N, Wu J, Gershwin E, Bowman EP, et al. Crosstalk among IL-23 and DNAX activating protein of 12 kDa-dependent pathways promotes osteoclastogenesis. J Immunol. 2015;194(1):316–24. [PubMed: 25452564]
47. Chiu YG, Shao T, Feng C, Mensah KA, Thullen M, Schwarz EM, et al. CD16 (FcRgammaIII) as a potential marker of osteoclast precursors in psoriatic arthritis. Arthritis research & therapy. 2010;12(1):R14. [PubMed: 20102624]
48. Xue J, Xu L, Zhu H, Bai M, Li X, Zhao Z, et al. CD14(+)CD16(−) monocytes are the main precursors of osteoclasts in rheumatoid arthritis via expressing Tyro3TK. Arthritis Res Ther. 2020;22(1):221. [PubMed: 32958023]
49. Mócsai A, Abram CL, Jakus Z, Hu Y, Lanier LL, Lowell CA. Integrin signaling in neutrophils and macrophages uses adaptors containing immunoreceptor tyrosine-based activation motifs. Nat Immunol. 2006;7(12):1326–33. [PubMed: 17086186]
50. Ortaldo JR, Winkler-Pickett R, Wigginton J, Horner M, Bere EW, Mason AT, et al. Regulation of ITAM-positive receptors: role of IL-12 and IL-18. Blood. 2006;107(4):1468–75. [PubMed: 16249390]
51. Colucci F Unexpected partnership between IL-15 and DAP10. Nat Immunol. 2007;8:1289. [PubMed: 18026080]

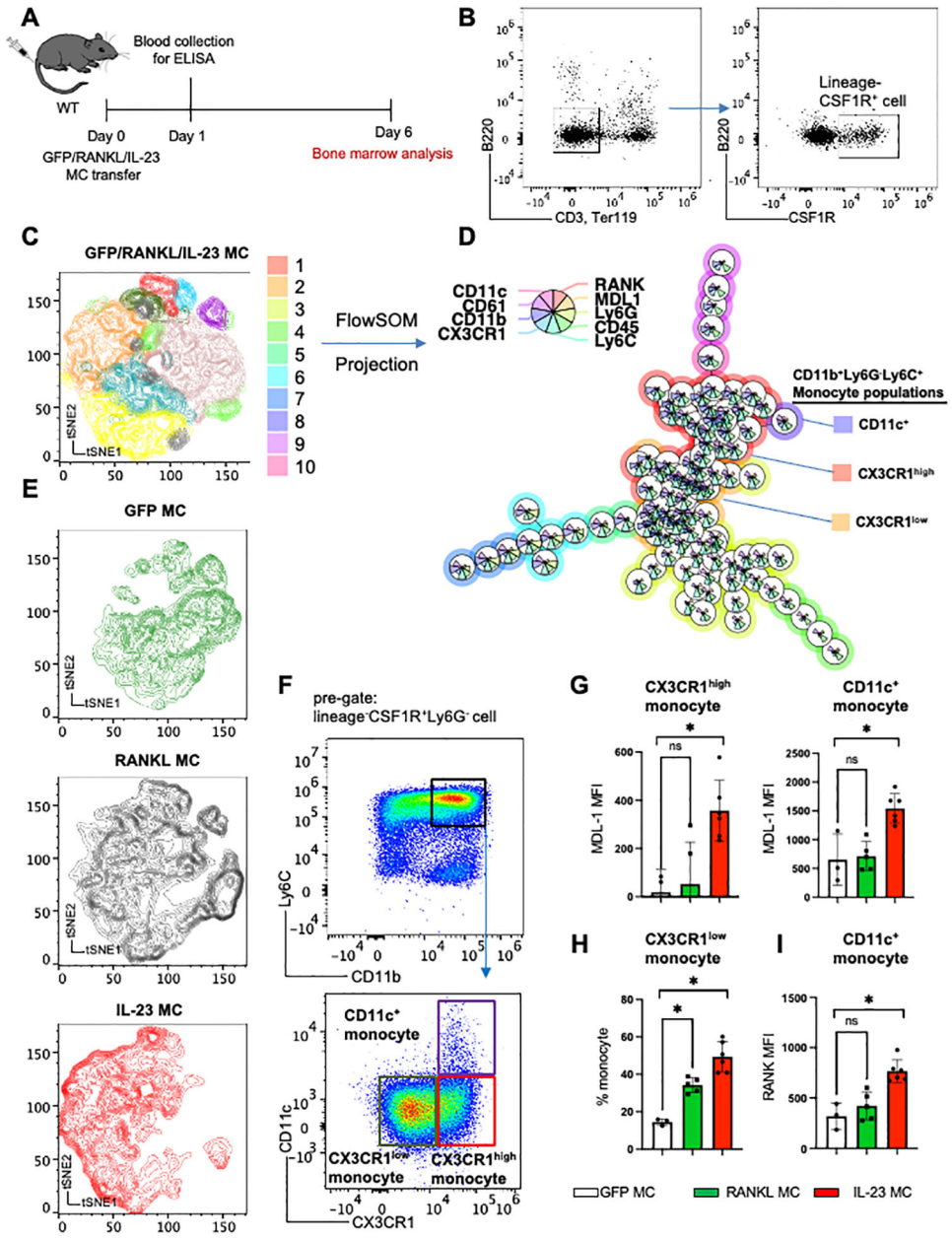

Figure 1: IL-23 induces the expansion of MDL-1^{+} osteoclast precursors.

(A) Schematic presentation of GFP (control)/RANKL/IL-23 MC transfer model in WT mice. **(B)** Representative figure of integrated flow cytometry data showing the gating strategy of lineage^{-}CSF1R^{+} cell used for unsupervised clustering with **(C)** tSNE plot and **(D)** FlowSOM based on expression levels of nine surface molecules, showing 10 distinct clusters. Size of each pie slices show the expression levels of each molecule. **(E)** Cell clusters post-GFP/RANKL/IL-23 MC gene transfer visualized in tSNE plot. **(F)** Representative gating strategy of three monocyte populations identified by FlowSOM, and **(G)** Mean Fluorescence Intensity (MFI) of MDL-1 among CX3CR1^{high} and CD11c^{+} inflammatory monocytes, **(H)** percentage of CX3CR1^{low} among CD11b^{+}Ly6G^{-}Ly6C^{+}monocyte populations, and **(I)** MFI of RANK among CD11c^{+}

monocyte population after GFP/RANKL/IL-23 MC transfer. Data represent mean ± SEM of single experiment. *P<0.05 by Mann-Whitney.

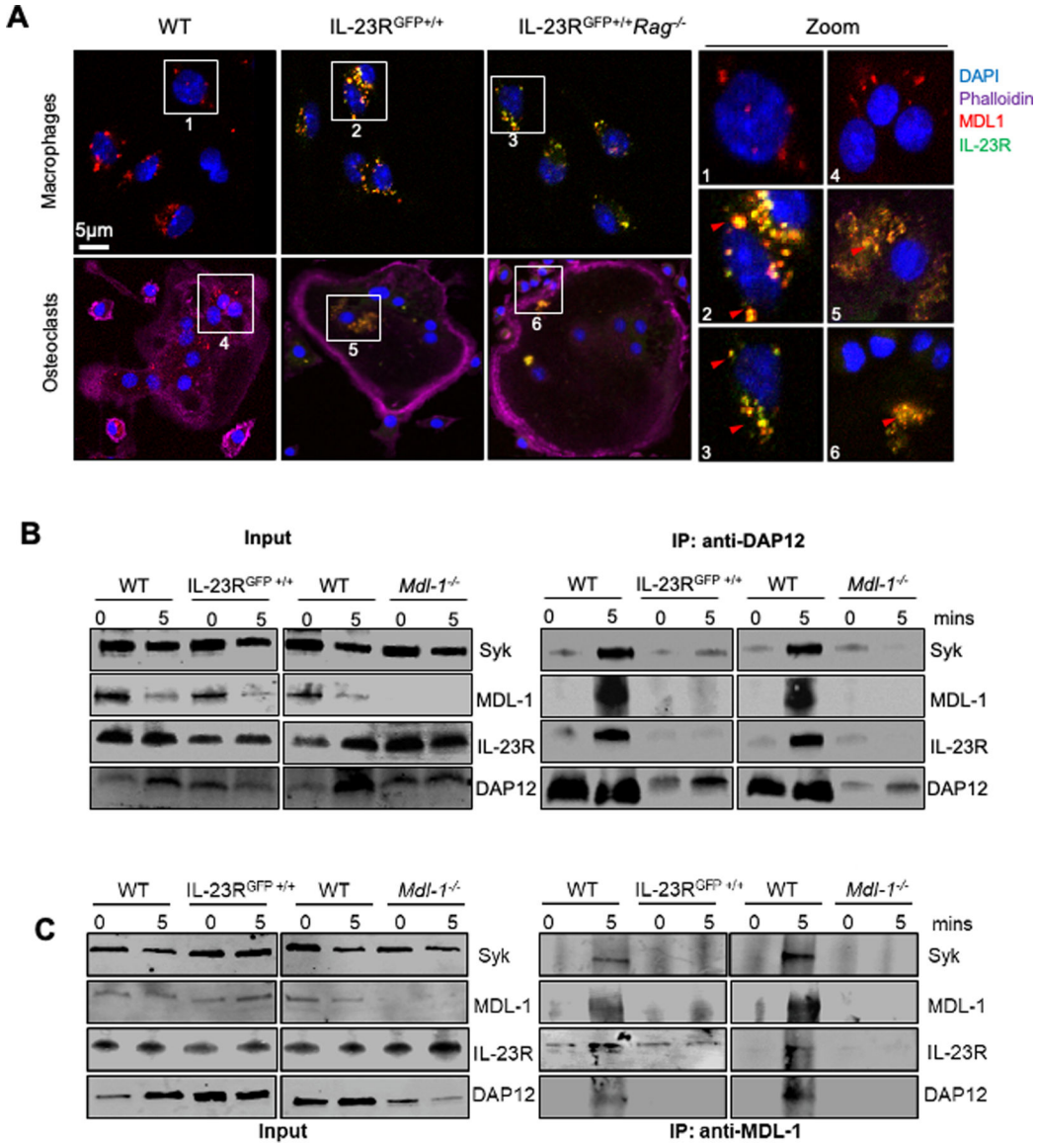

Figure 2: IL-23 activates inflammatory DAP12 signaling in MDL-1^{+} IL-23R^{+} double positive cells.

(A) Confocal microscopy images of bone marrow derived macrophages from WT, IL-23R$^{GFP+/+}$ and IL-23R$^{GFP+/+}$*Rag*$^{-/-}$ mice stained with MDL-1 (anti-MDL-1-PE-Cyan), IL-23R (anti-GFP-FITC-Green), nucleus (DAPI-blue), and actin (DyLight 650-Phalloidin) showing MDL-1 and IL-23R co-localization (yellow) in macrophages and osteoclasts. Images are representative of three independent experiments. (**B**) Immunoprecipitations of DAP12 and/or **(C)** MDL-1 with total cell lysates of WT, IL-23R$^{GFP+/+}$ and *Mdl-1*$^{-/-}$ derived BMMs stimulated with mouse rIL-23 (100 ng/ml) for 0, 5 mins, and immunoblotted with indicated antibodies showing DAP12 co-immunoprecipitation with MDL-1, IL-23R, STAT3, and SYK in WT lysates and lack of binding with DAP12 in either IL-23R$^{GFP+/+}$ and *Mdl-1*$^{-/-}$ BMMs.

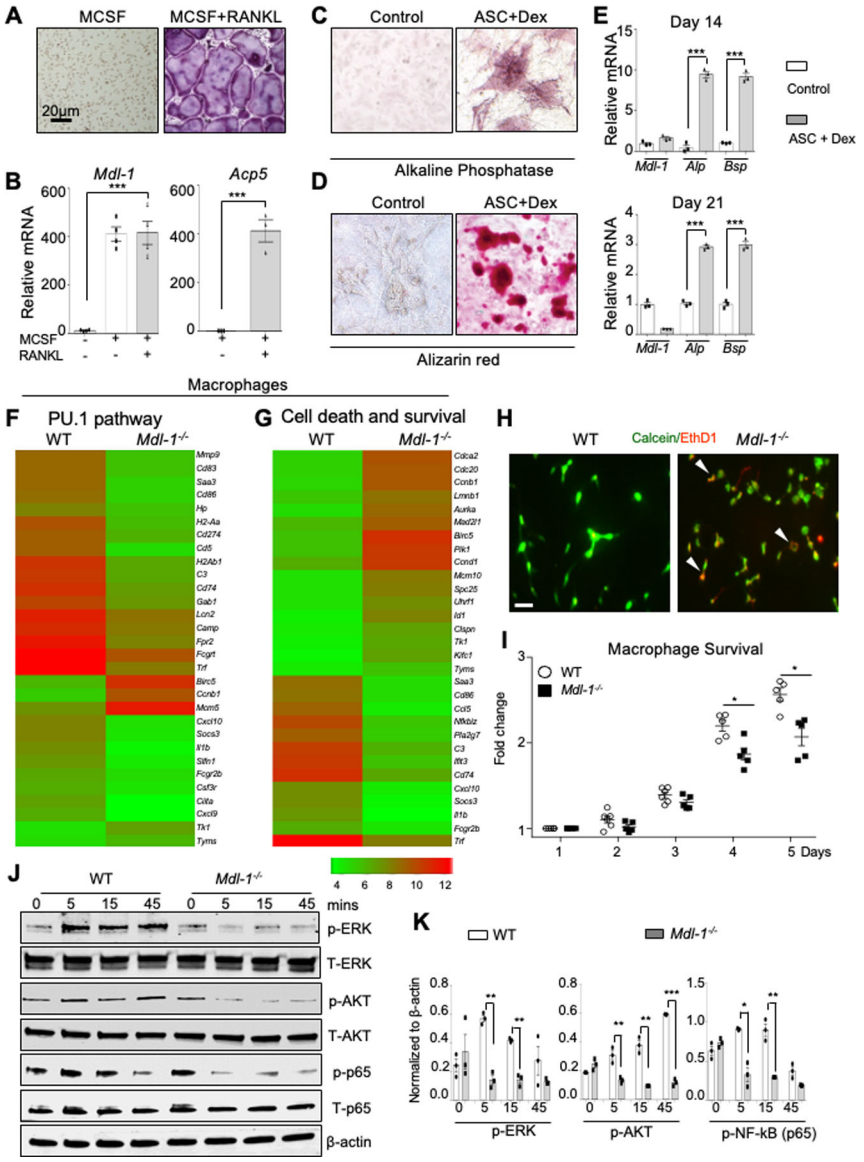

Figure 3: MDL-1 regulates the myeloid PU.1 transcriptional program in RANKL signaling.

(**A**) TRAP staining of WT bone marrow derived cells cultured in indicated showing increased expression of (**B**) *Mdl*-1 and *Acp5* during osteoclastogenesis. (**C**) Alkaline phosphatase (ALP) staining of nodules and (**D**) Alizarin red staining on 21 day cultures of calvaria-derived cells treated with ascorbic acid (ASC), β-glycerophosphate and dexamethasone (Dex) showing induction of osteoblast maturation and (**E**) expression of osteoblast differentiation markers independently of *Mdl-1.* (**F-G**) Hierarchical cluster analysis of selected genes with > 2-fold changes involved in (**F**) PU.1 pathway, (**G**) cell death and survival from microarray analysis of WT (n=9) and *Mdl-1*$^{-/-}$ (n=9) bone marrow cell stimulated with MCSF for 4 days. (**H**) Images of live/dead (Calcein/EthD1) staining and (**I**) fold change of macrophage survival (AlamarBlue assay) showing a lower survival rate of *Mdl-1*$^{-/-}$ macrophage. (**J**) Total cell lysates of WT and *Mdl-1*$^{-/-}$ derived BMMs stimulated with mouse rIL-23 (100 ng/ml) for indicated times, immunoblotted with indicated antibodies

and (**K**) protein band density showing significant differences of Erk, Akt, and NF-κB (p65) phosphorylation in *Mdl-1*$^{-/-}$ macrophages post-treatment. Data represent mean ± SEM of three independent experiments. **P*<0.05; ** *P*<0.01; *** *P*<0.001 by Mann-Whitney.

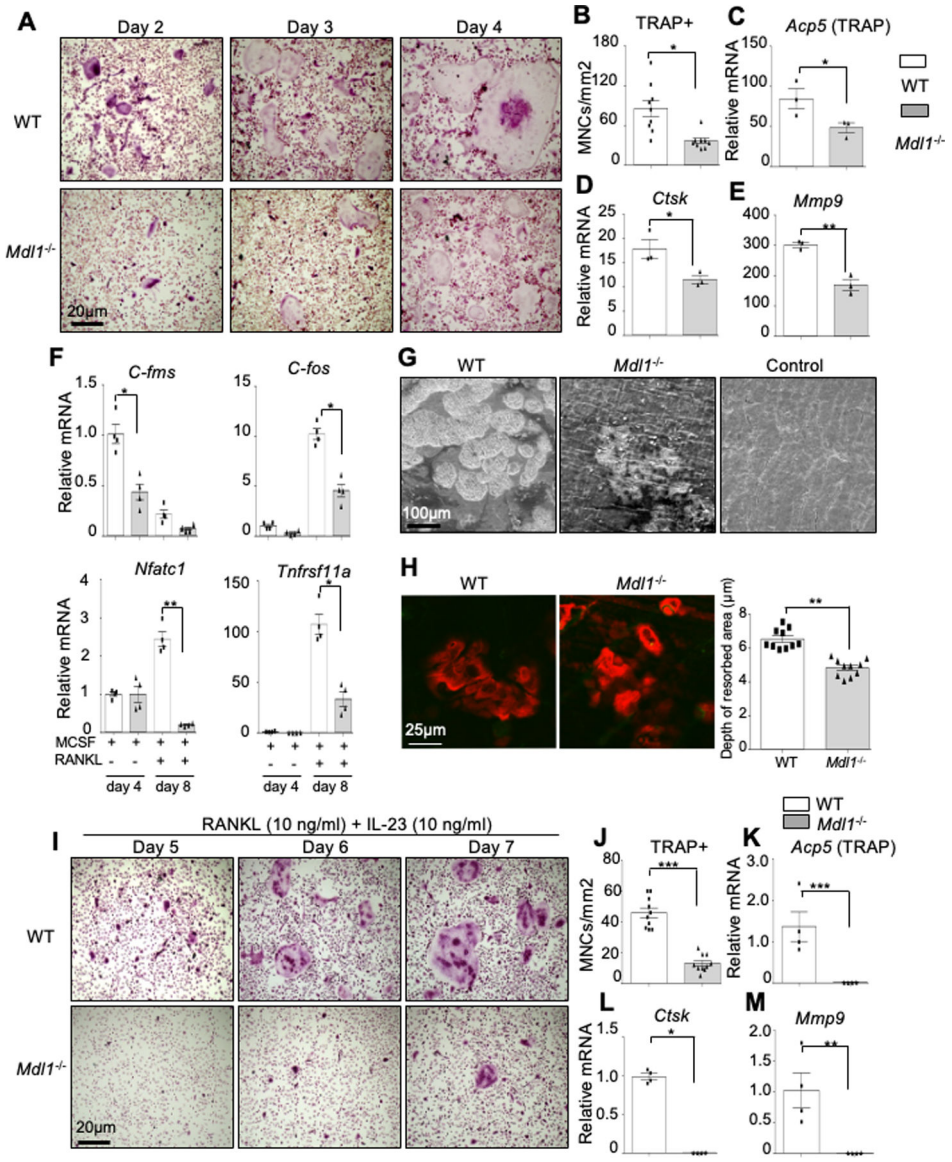

Figure 4: MDL-1 deficiency impairs osteoclast differentiation and bone resorption.

(**A**) TRAP stain of WT (n=4) and *Mdl-1*$^{-/-}$ (n=4) BMM cultured with MCSF and RANKL for indicated days showing delayed osteoclast maturation and (**B**) lower total number of TRAP^{+} multinucleated cells (MNCs) in *Mdl-1*$^{-/-}$ mice. Images are representative of three independent experiments. (**C-E**) Gene expression analysis showing reduced expression of osteoclast differentiation markers at day 6 and (**F**) osteoclast precursor at early (day 4) and late (day 8) time-point in *Mdl-1*$^{-/-}$ mice. (**G-H**) WT and *Mdl-1*$^{-/-}$ bone marrow cells cultured on dentine slices for 18 days with MCSF and RANKL showing **(G)** reduced dentine erosion surface area and **(H)** reduced depth of resorbed area by *Mdl-1*$^{-/-}$ osteoclasts. **(I)** TRAP stain of WT and *Mdl-1*$^{-/-}$ BMM cultured with MCSF, RANKL and IL-23 for indicated days showing delayed osteoclast maturation under inflammatory condition and **(J)** lower total number of TRAP^{+} MNCs in *Mdl-1*$^{-/-}$ mice. Images are representative of three independent experiments. **(K-M)** Gene expression analysis showing reduced expression of

osteoclast differentiation markers in *Mdl-1*$^{-/-}$ mice. Data represent mean ± SEM of two independent experiments. **P*<0.05; ** *P*<0.01; *** *P*<0.001 by Mann-Whitney test.

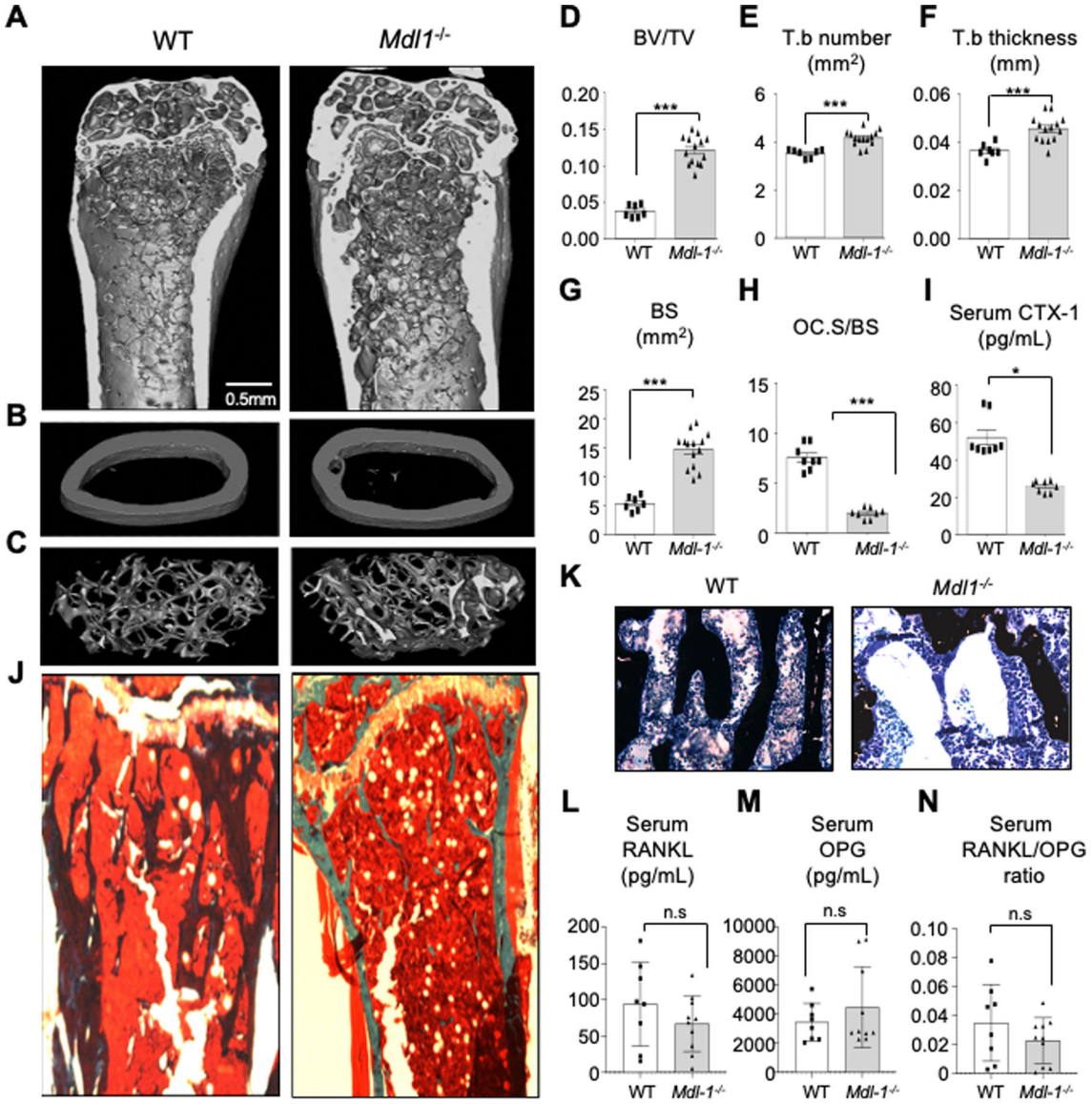

Figure 5: MDL-1 deficiency impairs osteoclast differentiation and bone loss *in vivo*.

(**A-G**) High resolution μCT analysis of 26-week old murine (**A**) femoral bone, (**B**) mid femur, (cortical bone) and (**C**) distal femur (trabecular bone) showing a significantly higher ratio of (**D**) the bone volume/tissue volume BV/TV, (**E**) Trabecular number, Tb.N, (**F**) Trabecular thickness, Tb.Th, (**G**) and Bone surface, BS (in *Mdl-1*$^{-/-}$ compared to WT mice. (**H**) Bone histomorphometry analysis showing lower osteoclast surface over bone surface area (Oc.S/BS), (**I**) lower type I collagen (CTX-1) serum levels (bone resorption marker) in *Mdl-1*$^{-/-}$, (**J**) Von Kossa-stain with (**K**) Toluidine blue counterstain showing increased calcium deposits in representative bone images. Serum analysis of **(L)** RANKL, **(M)** OPG and **(N)** ratio of RANKL/OPG levels showing no significant changes between WT and *Mdl-1*$^{-/-}$ mice. Data represent mean ± SEM of two independent experiments. *P<0.05; ** P<0.01; *** P<0.001 by Mann-Whitney test.

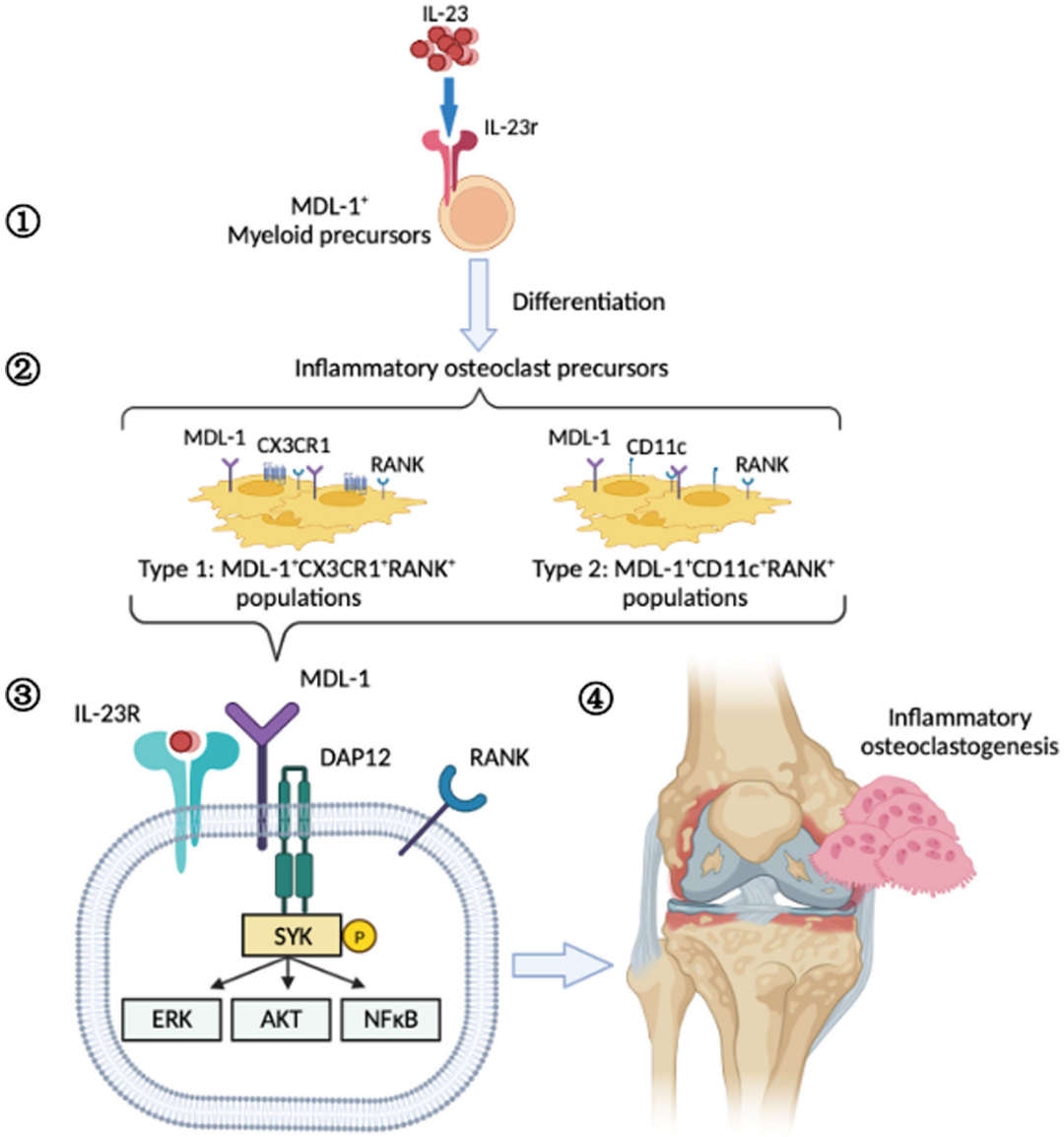

Figure 6: Schematic of IL-23 activation of MDL-1$^+$ osteoclast precursors in inflammatory arthritis.

Graphical representation of IL-23 effect on the (1) expansion of MDL-1$^+$IL-23r$^+$ myeloid precursors which (2) differentiate into MDL-1$^+$CX3CR1$^+$RANK$^+$ and MDL-1$^+$CD11c$^+$RANK$^+$ inflammatory osteoclast precursors resulting in (3) enhancement of DAP12-costimulatory signaling, (4) and terminal differentiation of osteoclasts contributing to pathogenicity in inflammatory arthritis.